Friction

Research Article

Study of lubricating nanocoatings for cardiovascular catheters based on molecular self-assembly and Schiff base reactions

Chengxiong Lin[1,2,3,✉], Huilu Yuan[3,4,5], Chengyong Wang[4,5,✉]

Cite this article: Lin CX, Yuan HL, Wang CY. *Friction* 2026, **14**: 9441201. https://doi.org/10.26599/FRICT.2025.9441201

ABSTRACT: During cardiovascular interventional surgeries, catheters come into mechanical contact with vascular tissues, resulting in friction, collisions, and compression that can damage the tissue. To address this, surface engineering is essential for modifying the catheter surface. Effective catheter coatings require high adhesion strength to prevent peeling or delamination from the inner surface, whereas the outer surface must provide excellent lubricity and biocompatibility. In this study, we used the layer-by-layer (LbL) technique to introduce catechol-modified chitosan (CC) and dopamine-modified oxidized hyaluronic acid (DOHA), which form a nanoscale, superhydrophilic, strongly adhesive, and biocompatible coating on cardiovascular catheters. Tight binding of CC and DOHA results from electrostatic interactions, chemical reactions, and catechol group enrichment, yielding an adhesion strength of up to 1 MPa. These CC/DOHA multilayers greatly enhance the lubrication performance of the TPU substrate, reducing the coefficient of friction (COF) by up to 95% compared with that of the uncoated state. After a 30-min friction test, the COF of the CC/DOHA$_{16}$ coating only slightly increased from 0.032 to 0.044, demonstrating excellent stability. Evaluations revealed a reduction in vascular intima damage from grade 5 without coating to grade 3, confirming the effectiveness of the coating in minimizing friction-induced damage.

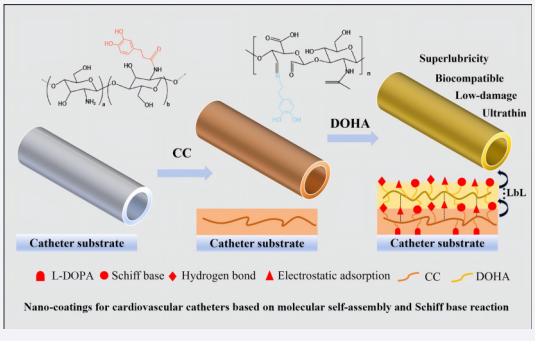

KEYWORDS: vascular catheter; layer-by-layer (LbL) adsorption; lubrication; adhesion strength

1 Introduction

Vascular interventional surgery uses specialized instruments, including catheters and guidewires, to treat cardiovascular diseases. This approach results in minimal trauma, high precision, a wide range of applications, simple operation, and quick recovery, making it the primary treatment for vascular diseases [1–4]. Among them, vascular interventional catheters refer to flexible hollow tubes that can be inserted into blood vessels. Currently, both the inner and outer layers of catheter materials are composed primarily of polymer materials [5], including polytetrafluoroethylene, polyethylene, polyamide, nylon, and polyvinyl chloride. These polymer materials are hydrophobic and generate considerable resistance when in contact with the complex vascular system, which may easily scratch the vascular tissue and cause mechanical friction-related damage [6–8]. Therefore, surface engineering is needed to modify catheter materials and reduce tissue injury [9–14].

Materials commonly used for surface lubrication modification of catheters include hydrophilic polymers. Examples include polyvinylpyrrolidone (PVP) [15], polyethylene glycol (PEG) [16], polyvinyl alcohol (PVA) [17], natural polysaccharides [18], and their composites [19]. When used as medical coatings, hydrogels typically have limited adhesion and stability to solid surfaces. This is especially true when fully expanded. As a result, hydrogel coatings may separate from the catheter surface. If this happens, their lubricating and biocompatibility effects are lost. Coating fragments may also cause tissue reactions, thrombosis, or serious adverse events such as myocardial embolism, thrombotic stroke, tissue necrosis, or death [20–24]. Studies have shown that the particle diameters affecting vascular embolism range from 15 to 200 μm. To prevent coating shedding, the catheter coating thickness should be kept below 15 μm [25]. Thus, improving the adhesion strength of coating materials and reducing their thickness have become key research focuses [26].

Methods for enhancing the adhesion strength of coatings can be learned from nature. Some marine organisms secrete proteins that allow them to adhere firmly to underwater surfaces. For

[1] Key Laboratory of Metallurgical Equipment and Control Technology (Ministry of Education), Wuhan University of Science and Technology, Wuhan 430081, China. [2] Hubei Key Laboratory of Mechanical Transmission and Manufacturing Engineering, Wuhan University of Science and Technology, Wuhan 430081, China. [3] Institute of Biological and Medical Engineering, Guangdong Academy of Sciences, Guangzhou 510316, China. [4] State Key Laboratory of High-Performance Tools, Guangdong University of Technology, Guangzhou 510006, China. [5] Guangdong Provincial Key Laboratory of Minimally Invasive Surgical Instruments and Manufacturing Technology, Guangdong University of Technology, Guangzhou 510006, China.

✉ Corresponding authors. E-mail: C. Lin, lcx3625@wust.edu.cn; C. Wang, cywang@gdut.edu.cn

Received: August 26, 2025; Revised: October 24, 2025; Accepted: December 3, 2025

example, mussels secrete mussel adhesive protein [27], sandcastle worms secrete Pc-1 adhesion proteins [28], and barnacles secrete cement proteins [29]. The catechol groups in these proteins are mainly responsible for strong adhesion. Therefore, small molecules with catechol groups, such as dopamine, tannic acid, and 3,4-dihydroxyphenylpropionic acid (dihydrocaffeic acid), are often used to make bioadhesive materials [30]. Wan et al. [31] modified hyaluronic acid with polydopamine to increase adhesion and grafted polyethylene glycol at different substitution levels. The grafting ratio of polyethylene glycol affects the coefficient of friction (COF) and frictional energy dissipation at the catheter-blood vessel interface. Song et al. [32] modified catheter and stent materials with dopamine and mucin, improving their wettability, wear resistance, and ability to inhibit cell adhesion. Song et al. [12] constructed high-density sulfobetaine zwitterionic polymer brushes on catheters using dopamine and sodium alginate as intermediate layers. These brushes achieved long-lasting lubricity ($\mu < 0.0078$) and, after 4 h of implantation in rabbits, exhibited no bioadhesion or thrombosis without the use of anticoagulants.

To reduce the coating thickness, Parada et al. [33, 34] created an ultrathin hydrogel coating on polyvinyl chloride tubes. In vitro and in vivo tests revealed that this coating reduced bacterial adhesion and prevented blood clot formation in the tubes. It does not affect blood coagulation ability. Electrostatic self-assembly is a fine coating technique. It achieves nanometer thickness through layer-by-layer (LbL) adsorption of oppositely charged polymers [35, 36]. Sunny et al. [37] prepared a nanoscale self-cleaning surface via LbL deposition of negatively charged silica nanoparticles and positively charged polyelectrolytes. Four or more LbL cycles created enough roughness to trap lubricant within the nanoporous coating. This provided a stable liquid interface that repelled water, low-surface-tension liquids, and complex fluids. Our group previously deposited polylysine/hyaluronic acid and chitosan/hyaluronic acid coatings on catheters via electrostatic self-assembly. This nanoscale coating significantly reduced the COF between the catheter and the vessel. Adding more layers further reduces arterial injury [38, 39]. However, the stability of nanocoatings cannot be directly and quantitatively measured. This ability is mainly judged indirectly by the stability of the liquid environment or anti-friction performance, thus demonstrating the safety and performance of the coatings.

In summary, creating an effective vascular catheter coating requires high adhesion strength to prevent peeling or delamination from the inner surface and good lubricity and biocompatibility on the outer surface. Consequently, designing a safe, ultrathin, low-damage, low-friction, and high-biocompatibility coating is crucial for reducing vascular injury and improving catheter materials. This study addresses these goals by grafting catechol groups onto the natural macromolecules chitosan (catechol-modified chitosan, CC) and hyaluronic acid (dopamine-modified oxidized hyaluronic acid, DOHA) to increase interfacial adhesion and multilayer stability. Building on LbL electrostatic self-assembly, we oxidize hyaluronic acid to aldehyde groups that react with the amino groups of chitosan via a Schiff base reaction, further optimizing the safety and stability of the coating. The resulting superhydrophilic, low-friction, and high-adhesion nanocoating for cardiovascular catheters (Fig. 1) aims to advance catheter modification for clinical application.

2 Materials and methods

2.1 Synthesis of CC and DOHA

Synthesis of CC. CC was generated by grafting 3,4-dihydroxyphenylacetic acid (HCA; Sigma-Aldrich, CAS number: 1078-61-1) onto chitosan (CHI; Sigma-Aldrich, CAS number: 9012-76-4) through an amide reaction. The detailed preparation steps were as follows [40]: 3.25 mmol of CHI was dissolved in 50 mL of 0.1 M dilute hydrochloric acid solution. The mixed solution was stirred evenly, and its pH was then adjusted to 4.5–5.0 with a NaOH solution. HCA (1.65 mmol) was subsequently dissolved in 6 mL of ultrapure water and added to the above solution. EDC (1.65 mmol) was dissolved in 50 mL of a 1:1 (v/v) mixture of ultrapure water and anhydrous ethanol and then added to the above mixture. The reaction mixture was stirred vigorously in the dark at room temperature for 10 h, and the pH was maintained between 4.5 and 5.0. Finally, the solution was subjected to dialysis via a dialysis bag (molecular weight cutoff of 3,500 Da) in an ultrapure water solution with a pH of 5.0 for 3 d. The product was freeze-dried and stored in a vacuum desiccator.

Synthesis of DOHA. The synthesis of DOHA involves two steps. First, hyaluronic acid (HA; Sigma-Aldrich, CAS number: 9067-32-7) was oxidized to convert the adjacent hydroxyl groups of HA into aldehyde groups. The carboxyl group of dopamine then reacts with the aldehyde group through a Schiff base reaction to graft the catechol group onto HA. Eventually, DOHA was obtained. The specific steps were as follows: 2.5 mmol of HA was

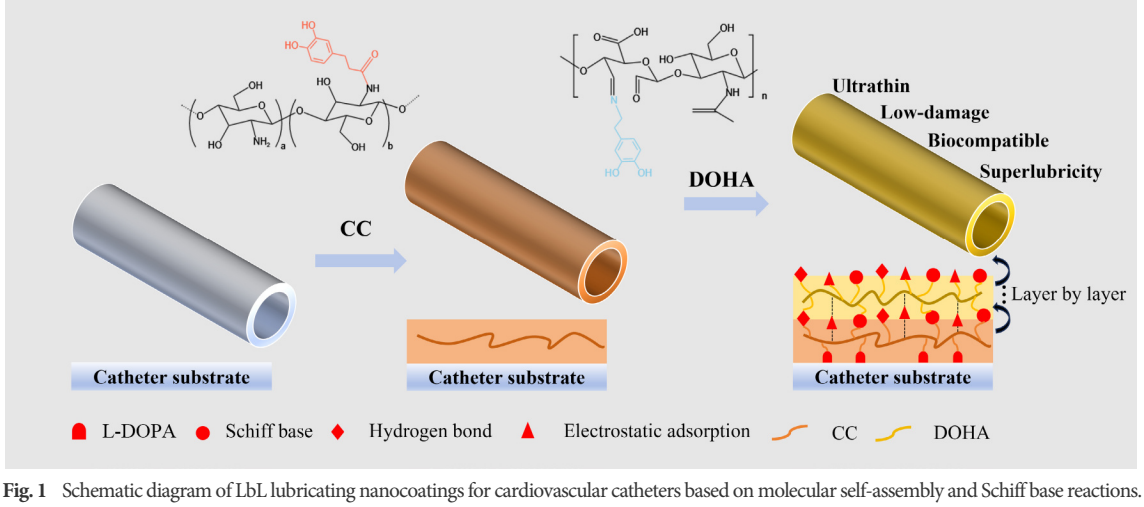

Fig. 1 Schematic diagram of LbL lubricating nanocoatings for cardiovascular catheters based on molecular self-assembly and Schiff base reactions.

dissolved in 100 mL of ultrapure water and stirred evenly to obtain a uniform solution with a concentration of 10 mg/mL. A total of 1.5 mmol of sodium periodate ($NaIO_4$; Sigma-Aldrich, CAS number: 7790-28-5) was dissolved in 5 mL of ultrapure water and then added dropwise to the HA solution with a molar ratio of $NaIO_4$ to HA of 3:5. After stirring in a dark environment at room temperature for 2 h, 0.5 mL of ethylene glycol was added to terminate the reaction. The solution was subjected to dialysis via a dialysis bag (8,000 Da) in an ultrapure water solution for 3 d, and the ultrapure water was replaced three times a day. Finally, the product of oxidized hyaluronic acid (OHA) was freeze-dried and stored in a desiccator.

Then, 40 mg of OHA was dissolved in 8 mL of PBS, and the pH was adjusted to 4.5–5.0 with hydrochloric acid. Then, 13.5 mg of 1-ethyl-3-(3-dimethylaminopropyl) carbodiimide hydrochloride (EDC; Sigma-Aldrich, CAS number: 1892-57-5) and 19 mg of dopamine (Sigma-Aldrich, CAS number: 62-31-7) were added, maintaining the pH at 5.0. The mixture was stirred at room temperature in the dark for 8 h. The product was dialyzed for 3 days in ultrapure water with a pH of 5.0 using a dialysis bag (3,500 Da) to remove unreacted substances. Finally, the DOHA product was freeze-dried and stored in a desiccator for further use.

Chemical structure characterization. Multiple methods were adopted to characterize and verify the material modifications, including Fourier transform infrared spectroscopy (FTIR Nexus 670, Thermo Nicolet, USA), hydrogen nuclear magnetic resonance (H-NMR, Avance NEO 400 MHz, Bruker, Germany), and ultraviolet-visible absorption spectroscopy (UV-Vis, Tecan, Switzerland), for the analysis of the material structure.

2.2 Multilayer (CC–DOHA) preparation

Coating preparation. Polyurethane (TPU) materials were first ultrasonically cleaned in anhydrous ethanol (EA) for 30 min and then transferred to a large amount of ultrapure water (UPW) for ultrasonic cleaning for 10 min. Finally, they were placed in an oven to dry for further coating treatment. Multilayer films were prepared on TPU by LbL self-assembly technology. Specifically, the pretreated TPU sheets were alternately immersed in CC and DOHA solutions at a concentration of 2 mg/mL for 10 min each to obtain positively and negatively charged film surfaces. Before the coating solution was changed, the TPU sheets were washed three times in UPW to remove the unabsorbed substances on the surface. The immersion adsorption-washing steps were repeated multiple times until the desired number of coating layers was obtained. The first layer of the film was immersed and adsorbed from CC, and the last layer ended with DOHA. After reaching the target number of coating layers, the material was immersed in EDC (5 mg/mL) at pH 4.5 for 30 min in the dark to allow the CC layer and DOHA layer to react fully and then washed with UPW. Finally, the material was naturally air-dried to obtain TPU materials with multilayer films (TPU@CC/DOHA).

Evaluation of the preparation process. To analyze the preparation process of CC/DOHA multilayer films, a quartz crystal microbalance (QCM-D, Biolin, Sweden) was used to monitor the construction process of the multilayer films in situ. The mass change on the sensor surface can be monitored by detecting the variation in the vibration frequency (F) of the quartz crystal, and the structural information of the surface can be obtained by tracking the dissipation factor (Q) [41]. Additionally, the electrostatic attraction between positive and negative charges ensures that the coating materials are closely and stably combined during the LbL self-assembly process. During this process, the structure and thickness of the coating can be precisely controlled, enabling the realization of specific functions and properties. Therefore, a zeta potential analyzer (Zetasizer Nano ZS90, Malvern, UK) was used to evaluate the charge characteristics of the materials and predict their behavior during the self-assembly process.

2.3 Evaluation of coating properties

Adhesion strength. The coating adhesion strength is used to evaluate the bond firmness between the coating and the base material. In the present work, a tensile peel test was conducted using a universal material testing machine to measure the interface adhesion strength between the coating and the TPU substrate. The test samples used for adhesion testing were prepared on two 10 mm × 10 mm TPU sheets. In the final step of coating deposition, the two sample surfaces were aligned and joined face to face. Notably, the materials of the last layer on the sheets are different, namely, CC and DOHA. A certain pressure was applied, and then the sheets were dried for the test. The tensile rate was 5 mm/min, and the test was carried out until the two sheets were pulled apart. The formula for calculating the bonding strength is as $\sigma = P/ab$. Here, σ represents the adhesion strength, P represents the tensile force, and a and b represent the length and width of the bonding area, respectively.

Surface characterization. The surface morphology of the coating was characterized by scanning electron microscopy (SEM, Phenom Scientific, the Netherlands) and atomic force microscopy (AFM, Dimension ICON, Bruker, USA). The hydrophilicity of the multilayers can be evaluated via a contact angle measuring instrument (DSA25, KRUSS, Germany). Additionally, the adhesion strength between the coating and the TPU substrate was evaluated via tensile peel tests on a universal material testing machine (34SC, Instron, USA). The test samples for adhesion testing were prepared by coating two 10 mm × 10 mm TPU thin sheets with each other. In the final step of coating synthesis, the two samples were joined face-to-face (with different charges on both sides) and then subjected to a certain pressure and drying before being used for the test. The tensile speed was 5 mm/min until the two samples were pulled apart. The formula for calculating the adhesion strength is as $\sigma = P/(ab)$, where σ represents the adhesion strength, P is the tensile force, and a and b are the length and width of the bonding area, respectively.

BC (biocompatibility). The blood compatibility of the coating materials was evaluated via a standard hemolysis test. The hemolytic suspension was prepared with whole blood (obtained from the National Engineering Research Center for Medical Devices Incubation Base, Guangzhou) for the standard hemolysis test. Because hemoglobin released from ruptured red blood cells has maximum absorption at a visible light wavelength of 416 nm, the degree of hemolysis of the test substances was determined via UV-Vis. The cell compatibility of the coating was analyzed via CCK-8 and live/dead cell double staining. Standard reagents (AbbKine) were used to test the cell viability on the 1st, 3rd, and 8th days of coculture with the coating. The absorbance (OD value) at a wavelength of 450 nm after CCK-8 incubation was measured via a multifunctional microplate reader. The cell state on the 3rd and 8th days of coculture with the coating was observed via a fluorescence inverted microscope.

2.4 Friction experiment

The aorta samples were obtained from the slaughterhouse within 2 h after death and sent to the laboratory. First, the mucosa and other tissues on the outer surface of the aorta were removed to ensure the sample's flatness. Then, samples were taken along the central axis of the aorta. The tissue samples for the friction

experiment were 50 mm × 30 mm in size, with a thickness of 1.5 to 3 mm for the aortic wall. The entire experiment was conducted within 4 h to avoid dehydration and deterioration. Sliding contact between the catheter and the blood vessel during cardiovascular catheterization was simulated in reciprocating sliding mode on a UMT-Tribolab (CETR, Bruker, USA). A polyurethane hemisphere (ϕ16 mm, D16H20, Lianpai Technology, China) was chosen as the counterpart of the aorta to mimic the materials commonly used for cardiovascular catheters. The friction hemisphere consisted of two parts: the front end featured a hemispherical friction head for the friction experiments, whereas the rear end was a metal part that connected the friction head to the friction testing machine. The prepared aorta sample was placed on silicon rubber and fixed with pins in a specially designed bath, as described in a previous publication [42]. To simulate real physiological conditions, a blood substitute solution was used in the friction experiment to create a vascular contact environment (90% volume of PBS solution and 10% volume of pig serum). In accordance with the suggestions of medical practitioners and previous studies, the normal load was 0.4 N, and the sliding speed was 5 mm/s. The friction force was measured for 5, 10, 15, 20, 25, and 30 min, with a sliding distance of 30 mm per cycle, at a sampling rate of 20 kHz.

2.5 Tissue damage evaluation

After the friction experiment, the porcine aorta tissue samples were transferred to paraformaldehyde solution at 4 °C. After 24 h of fixation, the samples were washed three times with PBS, immersed in PBS, and stored in a 4 °C refrigerator for subsequent damage characterization studies.

Fluorescence staining. DAPI (4',6-diamidino-2'-phenylindole dihydrochloride, Aldrich, CAS: 28718-90-3) and ConA (Concanavalin A, Aldrich, CAS: 11028-71-0) were used to stain the cell nuclei and glycoproteins on the vascular endothelium, respectively. The operation steps were as follows: (1) wash the tissue with PBS solution to remove excess paraformaldehyde solution; (2) add a mixture of ConA (2 mg/mL) and DAPI (2 mg/mL), submerge the tissue sample, and incubate in the dark for 30 minutes; (3) wash the tissue sample with PBS three times, each for 10 minutes; (4) use different light sources to excite ConA and DAPI, observe the fluorescence of the vascular tissue sample under an inverted fluorescence microscope (IX73 Olympus, Japan); and (5) use ImageJ software to statistically analyze the number of cell nuclei and the fluorescence intensity of glycoproteins on the tissue surface.

Surface morphology. The surface morphology of the tissue samples, both before and after the friction test, was observed by SEM (Phenom Prox, the Netherlands). The operation steps were as follows: (1) The friction area and nonfriction area of the vascular tissue were cut; (2) the samples were soaked in ethanol solutions of 50%, 70%, 80%, 90%, 95%, and 100% for gradient dehydration; (3) the dehydrated tissues were placed in a well-ventilated area for drying for more than 1 h; (4) the dehydrated and dried tissue samples were placed in a vacuum environment for gold spray treatment; (5) the samples were observed and photographed via SEM; and (6) ImageJ software was used to statistically analyze the diameters of the curled-up tissues on the surface.

Tissue sections. Changes in the cell nuclei, elastic fibers, and collagen fibers of vascular tissue can be observed through H&E (hematoxylin & eosin) staining and EVG staining. In EVG staining, elastic fibers are stained black, whereas collagen fibers are stained red. The steps for tissue section staining were as follows: First, the tissue samples were cut into thin slices approximately 3 mm in width; then, after routine dehydration, embedding, sectioning, mounting, dewaxing, and other treatments, the tissue sections were stained with H&E and EVG according to the operation steps in the user manuals; after staining, the tissue sections were sealed for long-term preservation; and finally, the tissue status of the sections was observed via a biological microscope (BX63, Olympus, Japan).

2.6 Data statistics

All the data are expressed as the means ± SDs. Differences between groups were determined via two-tailed Student's t test, with significance accepted at $p < 0.05$.

3 Results

3.1 Characterization of DOHA

HA, a naturally occurring substance present in the human body, has good biocompatibility. However, owing to its low stability in its natural state and easy degradation, HA often requires modification when used as a biomaterial. In the present work, the less reactive ortho-hydroxyl groups on HA were first oxidized to more reactive aldehyde groups to obtain OHA. OHA has highly reactive dialdehyde groups, providing grafting sites for dopamine (DOPA). Through the Schiff base reaction, DOPA subsequently reacts with the aldehyde groups on OHA. Finally, DOHA was synthesized (Fig. 2). Compared with those of the HA raw materials, the DOHA samples presented new absorption peaks at 1,716 and 1,530 cm^{-1}. OHA showed an absorption peak at 1,716 cm^{-1} attributed to the ester group (C=O), whereas DOHA presented a new absorption peak at 1,530 cm^{-1} belonging to C=C, indicating the successful synthesis of DOHA (Fig. 2(a)). Additionally, OHA exhibited a new proton absorption peak at 5.0 ppm, which is characteristic of the formation of a hemiacetal from the combination of an aldehyde group and a hydroxyl group. A comparison of the DOHA spectrum revealed a proton peak of the benzene ring of the catechol group in the range of 6.5 to 7.0 ppm, which is consistent with the characteristic peak at the same position in the ^{1}H-NMR spectrum of DOPA (Fig. 2(b)). Additionally, UV-Vis analysis revealed a significant absorption peak at 280 nm for the catechol group (Fig. 2(b)). Therefore, the water solutions of HA and OHA did not show absorption peaks in the spectral range. In contrast, the water solutions of DOPA and DOHA displayed prominent single absorption peaks at 280 nm. No additional absorption peaks were observed above 320 nm, indicating that the catechol group on DOHA did not undergo self-polymerization or oxidation (Fig. 2(c)). Accordingly, the successful synthesis of DOHA was confirmed from multiple perspectives through various detection methods.

Furthermore, since the catechol group plays a crucial role in interfacial adhesion, quantitative characterization of the DOHA grafting rate is vital. Given that the catechol group has a characteristic absorption peak at 280 nm, a standard curve of absorbance versus concentration can be established by preparing DOPA solutions of different concentrations (Fig. 2(d)). Water standard solutions of DOPA at concentrations of 0.01, 0.04, 0.07, 0.1, and 0.13 mg/mL were prepared. The absorbance of these five standard solutions at 280 nm was measured, and a standard curve was obtained through linear fitting ($A = 15.2C_1 + 0.01093$, $r = 0.9997$; C_1 represents the concentration of DOPA in water (mg/mL), and A represents the absorbance of the standard solution at 280 nm). The synthesized DOHA was dissolved in ultrapure water, and its absorbance at 280 nm was measured via a UV-Vis spectrometer. The grafting rate (GR) of DOPA in DOHA

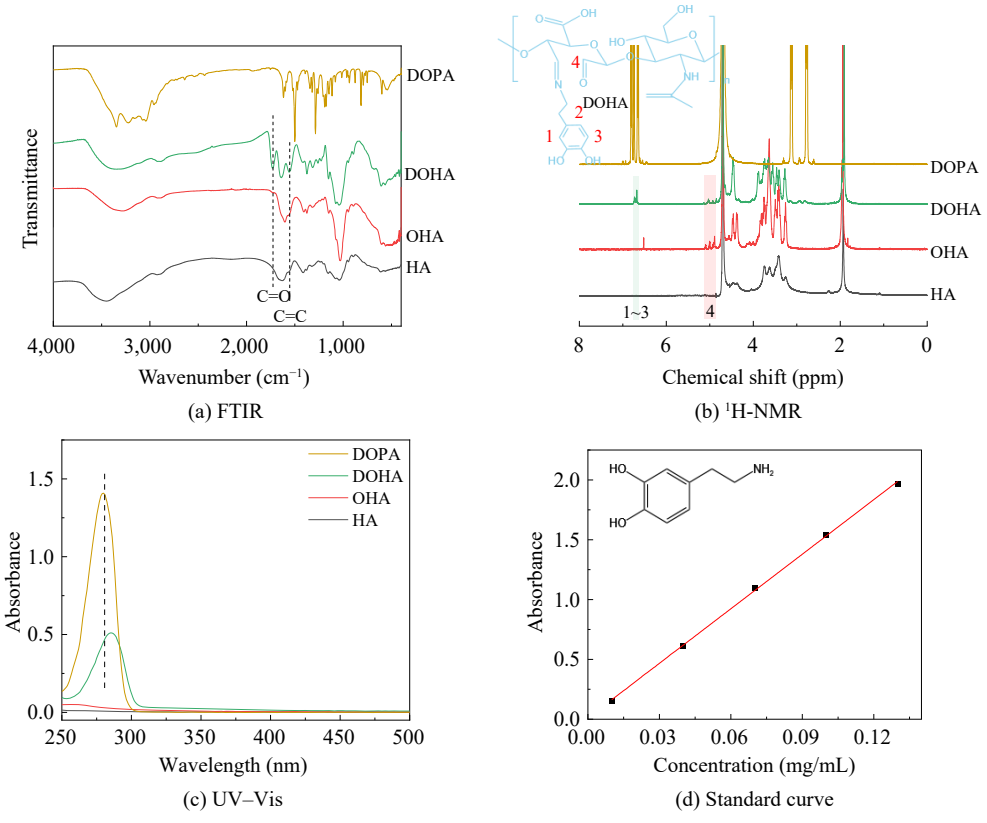

Fig. 2 Characterization of DOHA synthetic materials: (a) FTIR, (b) ^{1}H-NMR, (c) UV–Vis, and (d) standard curves of DOPA concentration.

is listed in Table 1.

3.2 Characterization of CC

CHI is the only abundant cationic basic amino polysaccharide in nature and features excellent antibacterial properties, biocompatibility, biodegradability, and anti-infective activity. In this study, the amino groups (–NH_2) reacted with HCA through amidation to successfully introduce catechol groups into the chitosan molecule, resulting in a grafted modified product, modified chitosan. This modification not only improves the solubility of CHI but also enhances its adhesion performance. The absorption peak of FTIR at 3,430 cm^{-1} corresponds to the stretching vibration of O–H, whereas the peaks at 1,635 and 1,599 cm^{-1} correspond to the stretching vibrations of the amide I and amide II groups of chitosan, respectively. The peaks at 1,077 and 1,033 cm^{-1} were typical C–O stretching vibrations in chitosan. A comparison of the CHI, CC, and HCA samples revealed that CC and HCA presented absorption peaks at 1,530 cm^{-1}, which is characteristic of aromatic C=C, whereas no such peak was observed for CHI (Fig. 3(a)). Furthermore, the ^{1}H-NMR spectra revealed that the proton peak of the main chain of chitosan could be observed at 3.6–4.0 ppm. The peaks at 6.7–7.0 ppm represented the proton peaks of the phenyl rings in the catechol groups (Fig. 3(b)). Additionally, both CC and HCA exhibited absorption peaks at 280 nm, whereas CHI did not. This indicated that the absorption peak at 280 nm was the characteristic absorption peak of the catechol group in HCA and CC, which is consistent with descriptions in the relevant literature [43, 44]. As a result, the successful synthesis of CC was verified through multiple testing methods from various perspectives.

In addition, taking advantage of the characteristic absorption peak of catechol groups at 280 nm, different concentrations of HCA were prepared to obtain a standard curve of the relationship between the absorbance and concentration (Fig. 3(d)). Five water

Table 1 The grafting rate of DOPA contained in DOHA and CC

Material	DOPA absorbance	DOPA concentration (mg/mL)	GR (%)
DOHA	0.42	0.027	5.78
CC	0.98	0.0577	5.41

standard solutions with HCA concentrations of 0.02, 0.04, 0.06, 0.08, and 0.10 mg/mL were prepared. The absorbances of these five standard solutions at 280 nm were measured via a UV-Vis spectrophotometer, and a standard curve was obtained through linear fitting ($A = 16.49C_2 + 0.03084$, $r = 0.9997$; C_2 represents the concentration of HCA in water (mg/mL), and A represents the absorbance of the standard solution at 280 nm). The synthesized CC was dissolved in ultrapure water, and its absorbance at 280 nm was measured via a UV-Vis spectrometer. GR of HCA in CC was calculated via the following formula, and the calculation results are listed in Table 1.

3.3 Characterization of CC–DOHA multilayers

To analyze the preparation process of the CC/DOHA multilayer film, QCM-D was used to monitor the in situ construction process of the multilayer film (Fig. 4). Before the experiment began, UPW was introduced until the instrument displayed a smooth baseline. First, a CC solution (2 mg/mL) was introduced, and the frequency (F value) immediately decreased, indicating that the substances were adsorbed onto the crystal wafer as the substrate. After 10 min of solution addition, the F value no longer decreased and remained stable, indicating that the adsorption of CC on the wafer surface had reached saturation and that the baseline was again leveled off. At this point, ultrapure water was introduced to rinse the wafer, and the F value increased, indicating that the wafer surface had lost weight and that the loosely adsorbed CC molecules had been washed away. After the samples were rinsed with ultrapure water, the F value leveled off again,

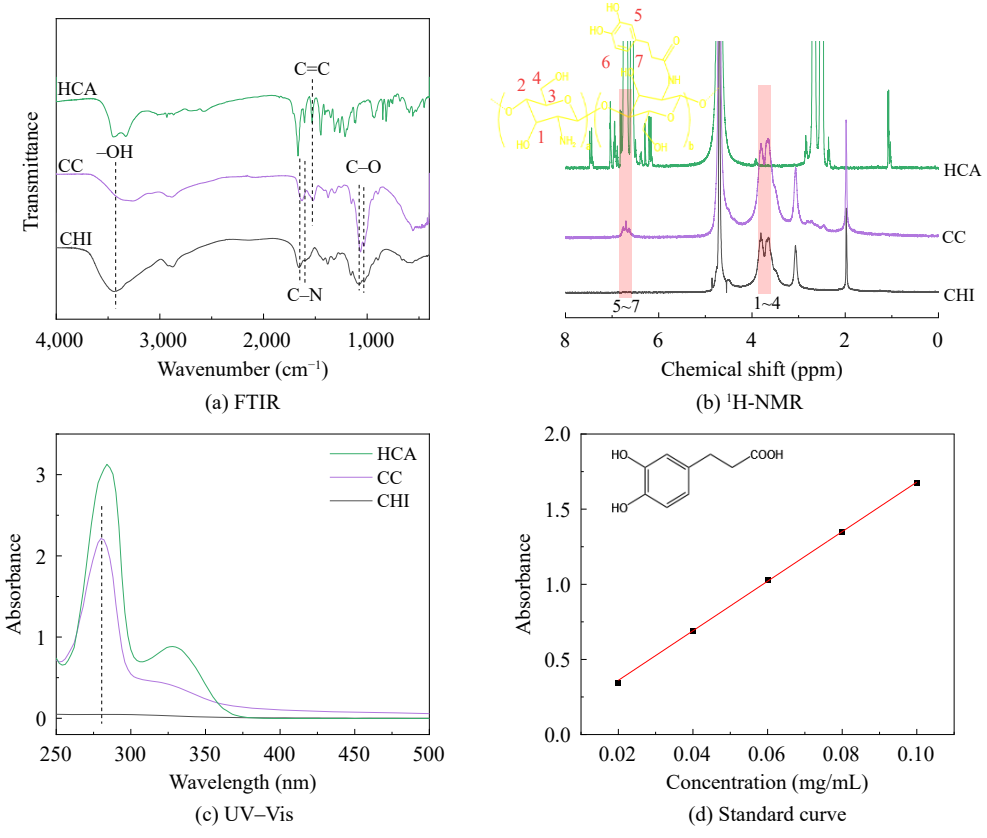

Fig. 3 Characterization of CC synthetic materials: (a) FTIR, (b) ^{1}H-NMR, (c) UV–vis, (d) standard curve of HCA concentration.

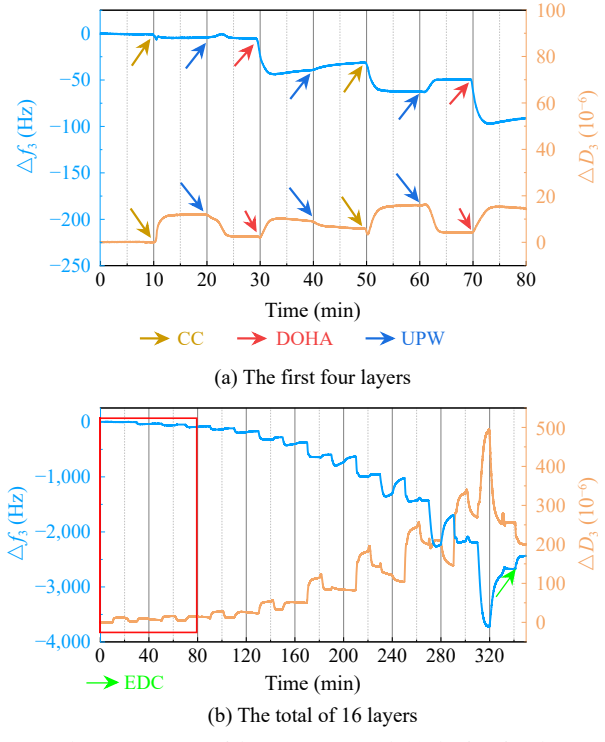

Fig. 4 Adsorption process of the coating material: (a) the first four layers and (b) a total of 16 layers.

indicating that the weight of the wafer surface did not change further and that no more CC molecules could be washed away, suggesting that some polycationic CCs were stably adsorbed on the wafer surface. Then, a polyanion DOHA solution (2 mg/mL) was introduced for 10 min, and the *F* value decreased again. DOHA was adsorbed onto the surface of the crystal, causing an increase in weight. The previous adsorption of CC introduced many positive charges. At this time, the negatively charged polyanion DOHA was adsorbed onto the crystal because of electrostatic forces and hydrogen bonds. After the adsorption amount of DOHA reached saturation, ultrapure water was introduced, causing the *F* value to rise, indicating weight loss, which suggests that the loosely adsorbed DOHA molecules were washed away with the water. When the *F* value stabilized again and no longer changed, the film was in a relatively stable state, and ultrapure water could no longer wash away the substances adsorbed on the film. At this point, the two-layer alternating film self-assembly was completed. Next, UPW, CC, UPW, and DOHA were alternately introduced for 10 min each. As the multilayer film was constructed, the frequency continuously increased in the negative direction (the mass continuously increased). As the number of layers increased, the negative frequency suddenly increased after the injection of DOHA, whereas the negative frequency suddenly decreased during the rinsing stage, indicating that the multilayer interface had reached a critical value. This occurred because the height of the sponge-like coating structure gradually increased as the number of deposition layers increased. In addition, the number of phenolic hydroxyl groups also increased. Therefore, the overall adsorption capacity of the coating continuously increased and reached a maximum at the 16th layer. After the electrolyte deposition was complete, an EDC solution with a pH of 4.5 was introduced to increase the bonding strength of the film during the reaction (340 min).

3.4 Characterization of coatings' properties

Figure 5 shows the AFM and SEM results of the TPU surface under different coating layers. As the number of coating layers increased, the TPU surface gradually became relatively smooth

and dense without cracks, and the uniformity of the coating surface improved layer by layer. Subsequently, AFM detection was carried out, and the TPU surface exhibited the same pattern, with enhanced surface uniformity. With increasing number of coating layers, the polymer film formed points, lines, and surfaces, eventually completely covering the surface, making it uniform and consistent. There was a slight undulation on the overall surface, with small protruding substances at certain positions, which may be related to the uneven distribution of the deposited polyelectrolyte. Through cross-sectional SEM observations, the thickness of the prepared 16-layer coating was approximately 150 nm. Additionally, the coating was closely bonded to the substrate without gaps, indicating that it had excellent cohesion and adhesion to the substrate.

As the number of surface coating layers increased, the contact angle gradually decreased (Fig. 6(a)). The results revealed that the hydrophilicity of the coating surface changed slightly when the number of coating layers was less than 8; when the number of coating layers reached 12, the change in hydrophilicity was more significant, and the contact angle fluctuated within a specific range. When the number of coating layers increased to 16, the contact angle decreased to 8°, approaching a superhydrophilic state. This change was related to the coverage and thickness of the coating on the substrate surface. The tensile test of surface coating adhesion conducted on the universal mechanical testing machine revealed that the tensile strength of TPU@CC/DOHA can reach 1 MPa (Fig. 6(b)). The addition of EDC can enhance the adhesion effect, confirming the role of EDC in the adhesion of self-assembled multilayer films and strengthening the bonding force between the coatings.

The hemocompatibility of the self-assembled coating was evaluated through an in vitro hemolysis test, and the results are shown in Fig. 6(c). The digital photos revealed that the control group and the TPU@CC/DOHA group presented a light yellow color similar to that of the physiological saline group, with red blood cells aggregating at the bottom of the EP tube and only slight hemolysis occurring. In contrast, the pure water group presented a uniform bright red color, indicating that the red blood cells had ruptured and that a severe hemolytic reaction had occurred. Because the hemoglobin released from ruptured red blood cells has maximum absorption at a visible light wavelength of 416 nm, the degree of hemolysis of the samples can be

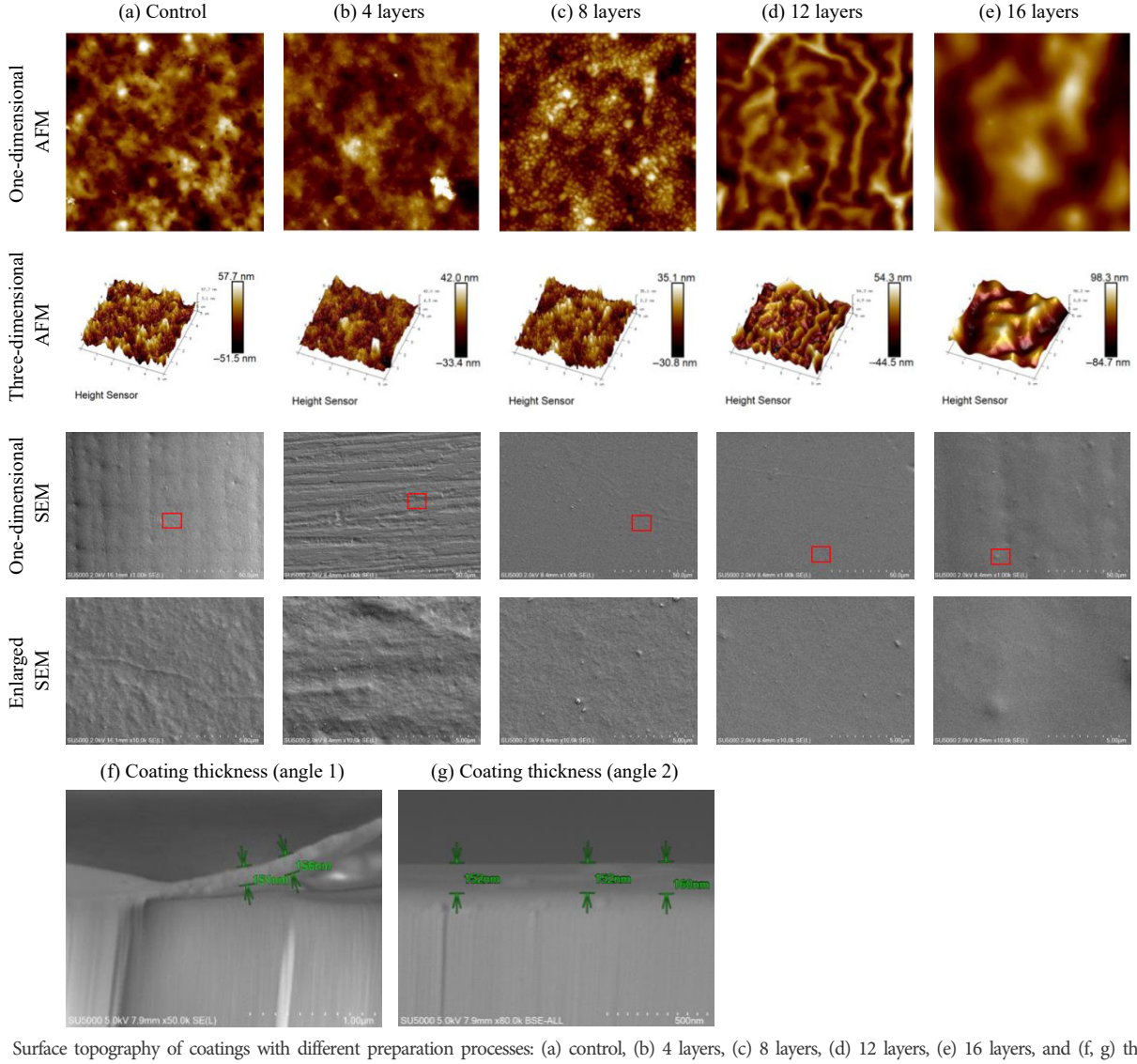

Fig. 5 Surface topography of coatings with different preparation processes: (a) control, (b) 4 layers, (c) 8 layers, (d) 12 layers, (e) 16 layers, and (f, g) thickness measurements. The samples are shown in the following order from top to bottom: one-dimensional AFM surface, three-dimensional AFM surface, one-dimensional SEM surface, and enlarged SEM surface in the red boxes.

清華大学出版社 Tsinghua University Press | SciOpen

quantitatively determined via UV–Vis spectroscopy (with 100% pure water). The experimental results revealed that the hemolysis rates of the control group and the TPU@CC/DOHA group were both less than 5%. The above results indicate that CC/DOHA has good hemocompatibility and can be safely used in in vivo applications.

Figure 6(d) shows the CCK-8 fluorescence intensity data of the cells from day 1 to day 8. On day 1, there was no significant difference in absorbance values among the groups; by day 3, the absorbance values of the TPU@CC/DOHA and TPU@CC/DOHA(E) groups were slightly greater, but there was no significant difference compared with those of the control group, indicating that the cell viability of these two groups was relatively high. By day 8, the viability of the control group was unstable, while the cells in the TPU@CC/DOHA and TPU@CC/DOHA(E) groups had better viability. Figure 6(e) presents the results of live/dead cell staining. After 3 days of culture, the cells in all the groups remained unspreading, with good viability and no dead cells, and there was no significant difference among the groups. By day 8, the cells in the control group and the coated groups had a normal morphology, were evenly spread, and exhibited ideal proliferation. The results of the CCK-8 and cytotoxicity tests indicated that the prepared coatings had good biocompatibility.

3.5 Characterization of lubrication properties

Figure 7 shows the COF and frictional energy dissipation for different frictional times. Frictional energy dissipation is the integral area of the friction force–displacement curve (*F*–*D*) [45]. The COF and energy dissipation remained stable within the first 10 min at relatively low levels (0.03 and 0.5 mJ, respectively), with no significant differences. However, the COF of the uncoated TPU friction head (Fig. 7(a)) began to increase linearly after 10 min, reaching 0.9 at 30 min; meanwhile, the friction energy dissipation increased from 0.5 to 10 mJ (Fig. 7(b)). In contrast, when the friction head was coated with eight layers, the COF rose slowly from 0.04 to 0.15 after 10 min, whereas the energy dissipation increased only slightly (from 0.5 to 3 mJ), with a limited change. Furthermore, the COF and energy dissipation of the friction head coated with 16 layers remained stable throughout the 30-min frictional period. Specifically, the COF was 0.06 for PU@CC/DOHA$_{16}$ and 0.05 for PU@CC/DOHA$_{16(E)}$. Therefore, within the limited coating range, the more layers of coating there are, the better the lubrication and antifriction effects.

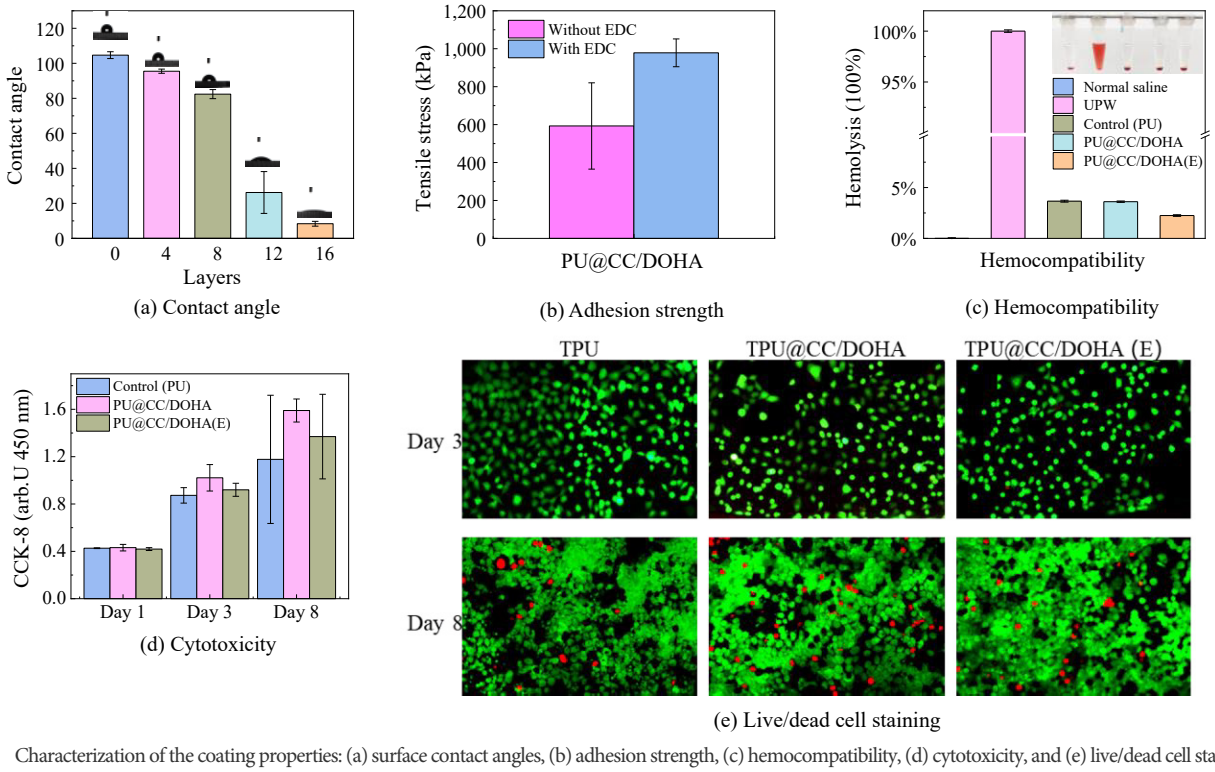

Fig. 6 Characterization of the coating properties: (a) surface contact angles, (b) adhesion strength, (c) hemocompatibility, (d) cytotoxicity, and (e) live/dead cell staining.

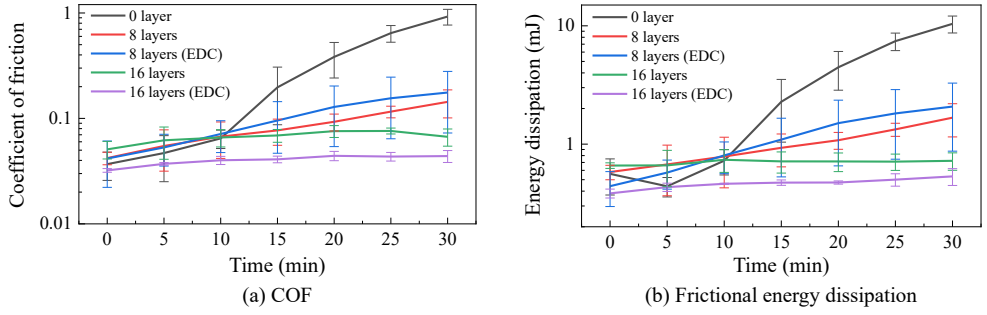

Fig. 7 (a) COF and (b) frictional energy dissipation of different coating layers in a single cycle (normal load of 0.4 N and sliding velocity of 5 mm/s).

3.6 Tissue damage analysis

Figures 8 and 9 show the tissue damage to the vascular surface before and after friction. After the uncoated TPU friction head slid on the aortic surface, the number of cell nuclei significantly decreased. Compared with the uncoated friction head, the TPU friction head coated with CC/DOHA multilayers displayed a greater number of cell nuclei after sliding on the aortic surface ($P < 0.05$). Similarly, the fluorescence intensity of extracellular glycoproteins on the aortic samples with the uncoated TPU friction head was different from that of the coated samples ($P < 0.05$). According to the SEM images, the surface of the original aorta appeared flat and intact, with no signs of wear or clear texture. After friction, all the samples were damaged to varying degrees. Among them, the inner membrane of the TPU friction head without a coating was severely damaged, with profound inner membrane rupture and curling. Additionally, a distinct fibrous network was observed on the surface of the blood vessel. In contrast, the samples with 8- and 16-layer coatings presented less damage. A statistical analysis of the size of the ruptured and curled inner membrane tissue (Fig. 9(c)) revealed that there was a significant difference between the TPU friction head without coating and the samples with surface coating treatment after friction ($P < 0.05$). Furthermore, the surface of vascular tissue may experience wear and shedding after friction. The more severe the wear is, the more significant the change in the thickness of the intima. The thickness of the intima in the cross-section of the blood vessel can be quantified through tissue sections. After friction with an uncoated TPU friction head, the surface endothelial cells were essentially destroyed and removed, and most of the collagen fibers in the subendothelial layer were stripped off, resulting in exposure of the elastic membrane and breakage of elastic fibers, resulting in a loose state. Figure 9(d) shows that the intima retention rate was less than 40%, while the intima retention rate of the coated TPU friction head reached 80%.

4 Discussion

As shown in Fig. 10, CHI and its modified material, CC, carried positive charges, whereas HA and its modified materials, OHA and DOHA, carried negative charges. Therefore, CC with a positive charge and DOHA with a negative charge were selected as the basic materials for coating synthesis, and they were alternately adsorbed through LbL to form a dense film. Second, the catechol groups were modified to simulate the firm adhesion of mussels, achieving adhesion at the coating–TPU and layer-layer interfaces. Moreover, the amino and hydroxyl groups in CC and the carboxyl and hydroxyl groups in DOHA formed hydrogen bond interactions, enhancing the cohesion of the coating. Additionally, the ungrafted amino groups in CC and the ungrafted aldehyde groups in DOHA undergo a Schiff base reaction, which introduces a covalent bond interaction to increase the adhesion between layers. Finally, soaking with EDC can promote the amide reaction between the ungrafted amino groups in CC and the carboxyl groups in DOHA, serving as a supplement to the Schiff base reaction, enhancing the covalent interaction of the coating and improving adhesion. As a consequence, the adhesion strength of CC/DOHA was greatly enhanced to 1 MPa (Fig. 6(b)) relative to 0.16 MPa (PLL-HA) and 0.56 MPa (PLL-

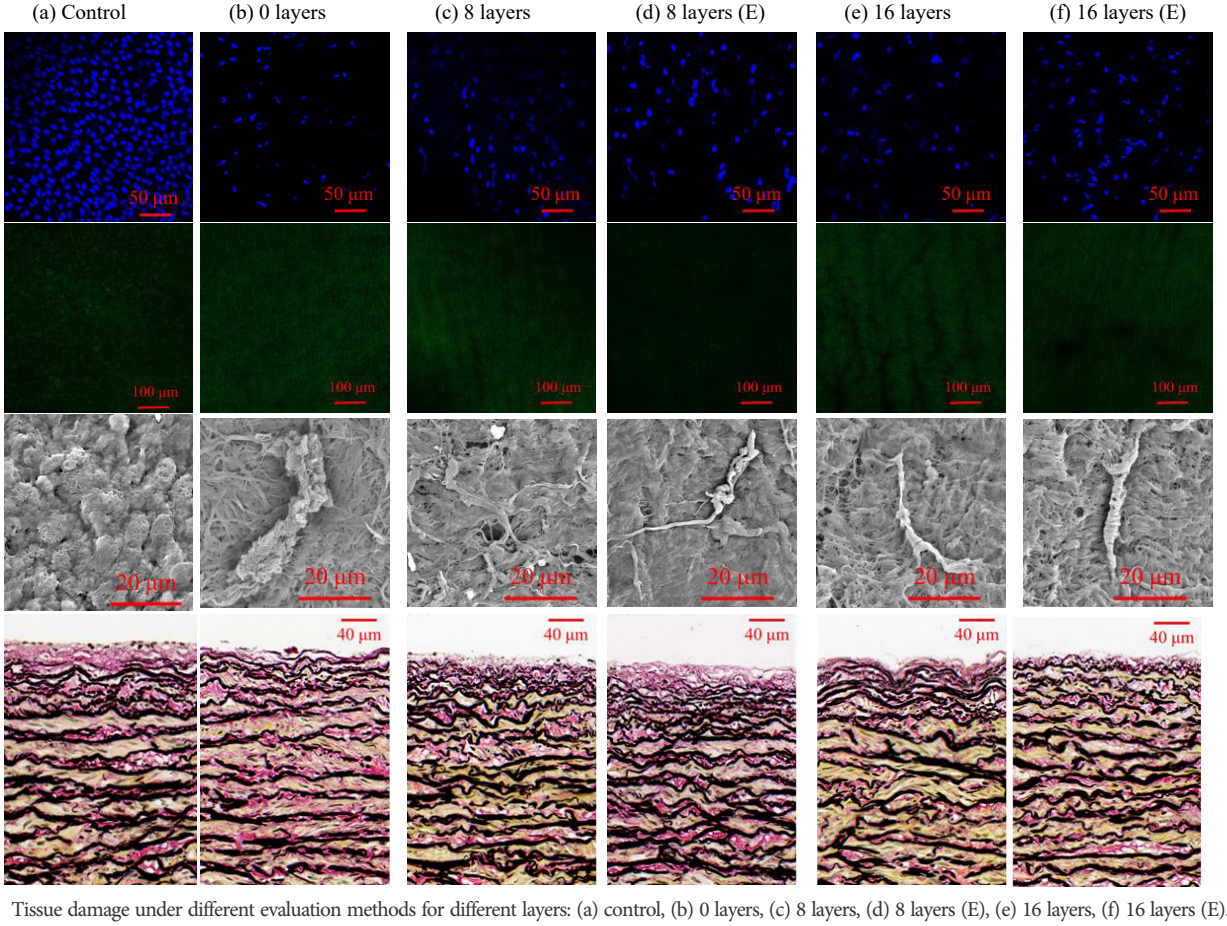

Fig. 8 Tissue damage under different evaluation methods for different layers: (a) control, (b) 0 layers, (c) 8 layers, (d) 8 layers (E), (e) 16 layers, (f) 16 layers (E). The samples are shown in the following order from top to bottom: DAPI staining, ConA staining, surface SEM topography, and sectional EVG staining.

HADN) [46], whereas it was lower than the results reported in other publications of a multilayer with a catechol group involved (2 MPa) [47, 48]. This might be due to the oxidation of the hydroxyl groups of HA to aldehyde groups, which sacrifices adhesiveness to a certain extent but enhances the stability of the LbL structure. In summary, the adhesion between the coating and the substrate, as well as the cohesion of the coating, were greatly enhanced by the synergistic effect of physical adsorption (electrostatic interaction, hydrogen bonding) and covalent bonding (Schiff base reaction, amide reaction). Additionally, the catechol groups gradually accumulated as the number of layers increased, resulting in a mussel-mimetic adhesion mechanism.

Additionally, to better evaluate the degree of damage to vascular tissues after friction, a damage assessment system was introduced in our previous research [42]. These methods include data standardization, the determination of subobjectives, the calculation of weight coefficients, and comprehensive evaluation scoring. Additionally, four forms of damage and their corresponding quantitative data were observed: endothelial cell shedding, surface tissue curling, intimal wear, and changes in surface glycoproteins. As a result, a detailed statistical analysis of multiple key indicators on the surface of vascular tissues was conducted in the present study. The results of the vascular intima damage scores after friction with different coatings are shown in Fig. 11. The friction head without a coating (0 layers) caused severe damage to the vascular intima after friction, with a damage score as high as 80%, indicating grade 5 damage. After coating, the degree of vascular intimal damage significantly improved, and the degree of intimal damage decreased to grade 3. This result fully demonstrated the effectiveness of the coating in reducing the damage to the vascular intima caused by friction during the process. Furthermore, the correlation analysis between the COF and the inner membrane injury score revealed a high correlation (Table 2), which is consistent with the relationship between the friction factor and tissue injury reported in Refs. [49, 50].

Compared with the uncoated state, the introduction of multiple layers significantly enhanced the lubrication performance of the TPU substrate, with a reduction in the friction coefficient of up to 95%. After a continuous friction test lasting 30 min, the COF of CC/DOHA$_{16}$ demonstrated excellent stability, increasing only

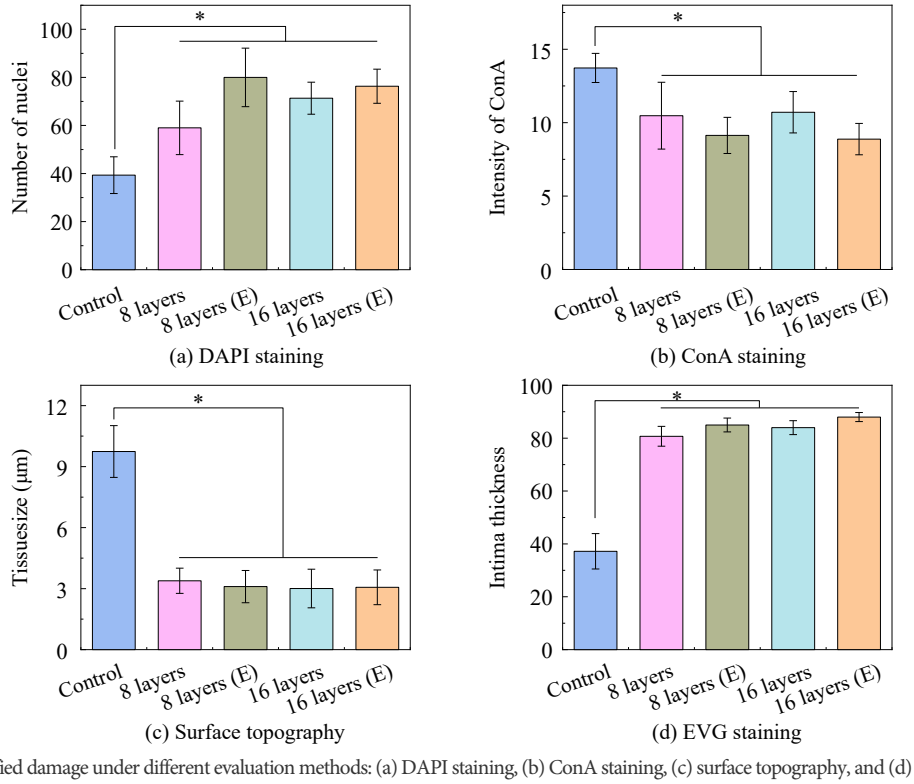

Fig. 9 Quantified damage under different evaluation methods: (a) DAPI staining, (b) ConA staining, (c) surface topography, and (d) EVG staining.

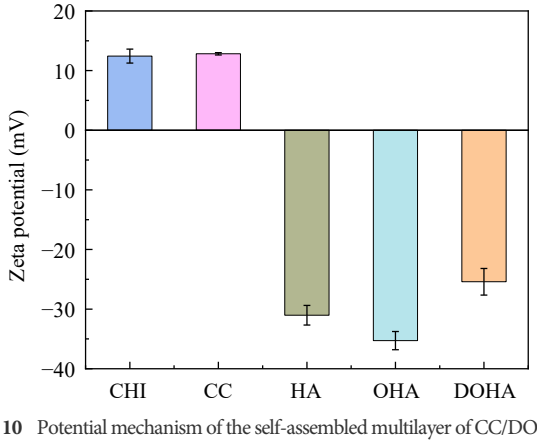

Fig. 10 Potential mechanism of the self-assembled multilayer of CC/DOHA.

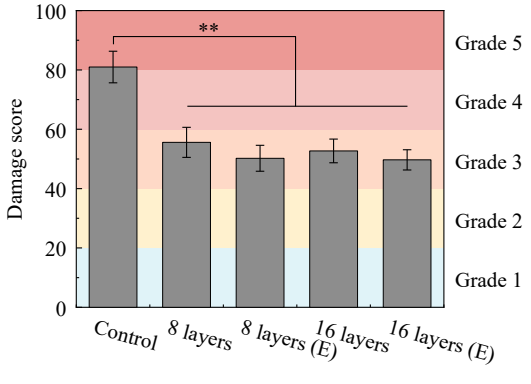

Fig. 11 Endothelial damage severity score (friction time, 30 min; normal load, 0.4 N; sliding velocity, 5 mm/s).

Table 2 Correlation coefficient analysis table

COF-damage score	Multilayer
P	0.0034 (**)
Correlation analysis	0.9800

slightly from the initial value of 0.032 to 0.044. It maintained a similar level of lubrication as the PLL-HA multilayers did [25] and was superior to the previous CHI-HADN multilayers [39]. This result indicated that the coating can effectively maintain a low-friction state and retain its lubrication performance even during prolonged friction. The CC/DOHA$_{16}$ multilayers with a sponge-like structure displayed superlubricity, enabling them to rapidly absorb a large amount of water in a liquid environment and form a hydration layer. This hydration layer not only endows the coating with the elasticity of a solid but also the fluidity of a liquid, thereby significantly improving its lubrication performance, as shown in Fig. 12. The superlubrication interface also reduced energy dissipation during the friction process and helped extend the service life of the coating. As mentioned in a previous publication, frictional energy dissipation is strongly correlated with the degree of mechanical damage to the tissue [42, 51]. During the reciprocating friction of the upper ball head on the vascular tissue, most of the kinetic energy is converted into thermal energy at the frictional interface, thereby causing tissue damage. As the number of layers of polyelectrolyte increased, the trends of frictional energy dissipation and the coefficient of friction were consistent, showing a negative correlation and indicating less mechanical damage. This finding is also consistent with the conclusion of Fig. 11. Furthermore, as the number of electrolyte layers continues to increase, the quantities of hyaluronic acid and catechol groups in the coating also continue to accumulate. The ability of these materials to adsorb and retain moisture is enhanced, continuously ensuring the wetting property of the coating [52]. In addition, the catechol groups in the coating can not only absorb water but also effectively adsorb the mucoprotein naturally present on the blood vessel surface [43]. This type of mucoprotein has good mechanical lubrication properties [25]. Therefore, the coating in the present study had a relatively typical ability to enhance lubrication.

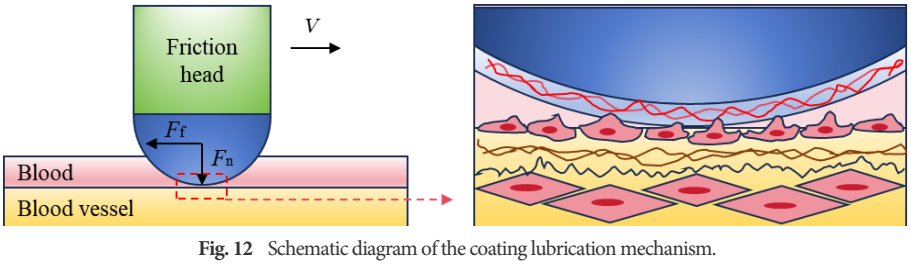

Fig. 12 Schematic diagram of the coating lubrication mechanism.

When the number of coating layers was 8 (4 layers of CC and 4 layers of DOHA), the COF tended to increase over time, particularly after 15 min. This phenomenon can be attributed to two main factors: (1) An insufficient number of coating layers resulted in inadequate hydrophilicity on the friction head, with a contact angle of 80°. The thickness of the hydration layer was relatively thin, and the coverage area was not extensive enough, restricting the elasticity of the coating on the friction head and the fluidity of the liquid, thereby increasing the COF. (2) An insufficient number of coating layers also affects the enrichment of catechol groups and hydrogen bonds, resulting in shedding of the coating, and the COF gradually increases over time. As the number of coating layers increased, both the hydrophilicity of the friction head surface and the degree of catechol group enrichment tended to increase.

5 Conclusions

On the basis of the natural macromolecules chitosan and hyaluronic acid, this work designed a hydrophilic lubricating coating and investigated its preparation mechanism, physical properties, biological properties, and lubricating and anti-friction performance. The conclusions were as follows:

(1) The CC and DOHA were successfully synthesized and verified through various detection methods.

(2) Ultrathin coatings of approximately 150 nm were prepared on the TPU by LbL deposition of CC and DOHA materials. Strong adhesion between CC and DOHA was achieved through electrostatic interactions, chemical reactions, and the presence of enriched catechol groups, with an adhesion strength of 1 MPa at the TPU-coating interface. With increasing number of coating layers, the hydrophilicity gradually increased, and a superhydrophilic state was reached at 16 layers.

(3) As the number of coating layers increased, the anti-friction effect gradually increased, with the maximum COF reduced by 95%, lowering the friction force from 0.5 to 0.03 N. During the 30-min friction test, the 16-layer coating demonstrated excellent lubrication stability. The EDC-enhanced multilayers played a specific role in reducing the COF and energy dissipation.

(4) The superlubricating interface (hydration layer) formed by the hydrophilic coating significantly reduced damage to the tissue surface. The damage evaluation system results revealed that the degree of vascular intima damage decreased from grade 5 without coating to grade 3, confirming the effectiveness of the coating in reducing vascular intima damage during the friction process.

Acknowledgements

This work was supported by the National Natural Science Foundation of China (52205186).

Declaration of competing interest

The authors have no competing interests to declare that are relevant to the content of this article.

References

[1] Guo J, Guo S X, Shao L, Wang P, Gao Q. Design and performance evaluation of a novel robotic catheter system for vascular interventional surgery. *Microsyst Technol* **22**(9): 2167–2176 (2016)

[2] Wang S, Liu Z, Tian L M, Bing W. Optimisation of photo-curable 3D-printed bionic double layer lower extremity vascular models based on biomechanical performance evaluation. *Biosurf Biotribol* **11**: e70003 (2025)

[3] Bonatti J, Vetrovec G, Riga C L, Wazni O, Stadler P. Robotic technology in cardiovascular medicine. *Nat Rev Cardiol* **11**(5): 266–275 (2014)

[4] Yuan H L, Lin C X, Wang C Y. Research progress of the interaction between blood vessels and intervention catheters and its surface modification. *Friction* **13**(7): 9441003 (2025)
[5] Tal M G, Ni N N. Selecting optimal hemodialysis catheters: Material, design, advanced features, and preferences. *Tech Vasc Interv Radiol* **11**(3): 186–191 (2008)
[6] Takashima K, Ohta M, Yoshinaka K, Washio T, Chinzei K. Methods for evaluating friction between intravascular device and vascular biomodel. *Tribol Online* **19**(1): 42–54 (2024)
[7] Xie D, Leng Y X, Jing F J, Huang N. A brief review of bio-tribology in cardiovascular devices. *Biosurf Biotribol* **1**(4): 249–262 (2015)
[8] Wang Z X, Wang K P, Xu Y. Friction injury of the central vein caused by catheter for hemodialysis: An in vitro study. *Sci Rep* **14**: 5836 (2024)
[9] Duta O C, Ţiţu A M, Marin A, Ficai A, Ficai D, Andronescu E. Surface modification of poly (vinylchloride) for manufacturing advanced catheters. *Curr Med Chem* **27**(10): 1616–1633 (2020)
[10] Zhang C N, Pan L P, Wang X J, Guo R, Zhao Y, Liang S Z. A radial micro-vibration system for reducing friction of passive interventional guidewire. *J Appl Phys* **137**: 014501 (2025)
[11] Wang J Y, Xu Y, Li S L, Tang L Y, Li X M, Song J, Liu Y H. Physical entanglement improves the anti-adsorption and super-lubricity properties of polyacrylamide-based hydrogels for biomedical applications. *Adv Compos Hybrid Mater* **8**(2): 208 (2025)
[12] Song X Z, Man J, Qiu Y H, Wang J L, Liu J N, Li R J, Zhang Y Q, Li J Y, Li J F, Chen Y G. High-density zwitterionic polymer brushes exhibit robust lubrication properties and high antithrombotic efficacy in blood-contacting medical devices. *Acta Biomater* **178**: 111–123 (2024)
[13] Guo W C, Zhao L J, Qin Z H, Wang Y G, Zhang H Y. Bioinspired self-adhesive coating for surface functionalization of medical devices with lubrication and antibacterial properties. *Friction* **13**(11): 9440926 (2025)
[14] Jia Y R, Zhang H Y. A hydrophilic lubricating coating with dual functions of antibacterial adhesion and urease-responsive bactericidal activity for urinary tract implantable devices. *ACS Appl Mater Interfaces* **17**(23): 33730–33744 (2025)
[15] Sun M, Wu Q Y, Xu J, He F, Brown A P, Ye Y M. Vapor-based grafting of crosslinked poly (N-vinyl pyrrolidone) coatings with tuned hydrophilicity and anti-biofouling properties. *J Mater Chem B* **4**(15): 2669–2678 (2016)
[16] Ding X, Yang C, Lim T P, Hsu L Y, Engler A C, Hedrick J L, Yang Y Y. Antibacterial and antifouling catheter coatings using surface grafted PEG-b-cationic polycarbonate diblock copolymers. *Biomaterials* **33**(28): 6593–6603 (2012)
[17] Yang S H, Lee Y J, Lin F H, Yang J M, Chen K S. Chitosan/poly (vinyl alcohol) blending hydrogel coating improves the surface characteristics of segmented polyurethane urethral catheters. *J Biomed Mater Res* **83B**(2): 304–313 (2007)
[18] Bračič M, Šauperl O, Strnad S, Kosalec I, Plohl O, Zemljič L F. Surface modification of silicone with colloidal polysaccharides formulations for the development of antimicrobial urethral catheters. *Appl Surf Sci* **463**: 889–899 (2019)
[19] Song X Z, Man J, Qiu Y H, Wang J L, Liu J N, Li R J, Zhang Y Q, Li J Y, Li J F, Chen Y G. Design, preparation, and characterization of lubricating polymer brushes for biomedical applications. *Acta Biomater* **175**: 76–105 (2024)
[20] Chopra A M, Mehta M, Bismuth J, Shapiro M, Fishbein M C, Bridges A G, Vinters H V. Polymer coating embolism from intravascular medical devices: A clinical literature review. *Cardiovasc Pathol* **30**: 45–54 (2017)
[21] Chopra A M, Rapkiewicz A, Daggubati R, Sequeira A, Hu Y C, Bhatt D L, Sharma S K, Cruz J P, Tzafriri A R, Edelman E R. Analysis: Intravascular devices with a higher risk of polymer emboli: The need for particulate generation testing. *Biomed Instrum Technol* **54**(1): 37–43 (2020)
[22] Mehta R I, Mehta R I, Choi J M, Mukherjee A, Castellani R J. Hydrophilic polymer embolism and associated vasculopathy of the lung: Prevalence in a retrospective autopsy study. *Hum Pathol* **46**(2): 191–201 (2015)
[23] Grundeken M J, Li X F, Kurpershoek C E, Kramer M C, Vink A, Piek J J, Tijssen J G P, Koch K T, Wykrzykowska J J, de Winter R J, et al. Distal embolization of hydrophilic-coating material from coronary guidewires after percutaneous coronary interventions. *Circ Cardiovasc Interv* **8**(2): e001816 (2015)
[24] Chen Z H, Zhang Y, Wang C Y, Chen B. Understanding the cutting mechanisms of composite structured soft tissues. *Int J Mach Tools Manuf* **161**: 103685 (2021)
[25] Lin C X, Kaper H J, Li W, Splinter R, Sharma P K. Role of endothelial glycocalyx in sliding friction at the catheter-blood vessel interface. *Sci Rep* **10**: 11855 (2020)
[26] Mehta R I, Mehta R I, Solis O E, Jahan R, Salamon N, Tobis J M, Yong W H, Vinters H V, Fishbein M C. Hydrophilic polymer emboli: An under-recognized iatrogenic cause of ischemia and infarct. *Mod Pathol* **23**(7): 921–930 (2010)
[27] Li L, Zeng H B. Marine mussel adhesion and bio-inspired wet adhesives. *Biotribology* **5**: 44–51 (2016)
[28] Zhang D H, Liu J J, Chen Q, Jiang W N, Wang Y B, Xie J Y, Ma K Q, Shi C, Zhang H D, Chen M Z, et al. A sandcastle worm-inspired strategy to functionalize wet hydrogels. *Nat Commun* **12**: 6331 (2021)
[29] Fan H L, Wang J H, Gong J P. Barnacle cement proteins-inspired tough hydrogels with robust, long-lasting, and repeatable underwater adhesion. *Adv Funct Mater* **31**(11): 2009334 (2021)
[30] Zhang H, Zhao T Y, Newland B, Liu W G, Wang W, Wang W X. Catechol functionalized hyperbranched polymers as biomedical materials. *Prog Polym Sci* **78**: 47–55 (2018)
[31] Wan H P, Lin C X, Kaper H J, Sharma P K. A polyethylene glycol functionalized hyaluronic acid coating for cardiovascular catheter lubrication. *Mater Des* **196**: 109080 (2020)
[32] Song J, Lutz T M, Lang N, Lieleg O. Bioinspired dopamine/mucin coatings provide lubricity, wear protection, and cell-repellent properties for medical applications. *Adv Healthc Mater* **10**(4): 2000831 (2021)
[33] Parada G A, Yuk H, Liu X Y, Hsieh A J, Zhao X H. Impermeable robust hydrogels via hybrid lamination. *Adv Healthc Mater* **6**(19): 1700520 (2017)
[34] Parada G, Yu Y, Riley W, Lojovich S, Tshikudi D, Ling Q, Zhang Y F, Wang J X, Ling L, Yang Y Y, et al. Ultrathin and robust hydrogel coatings on cardiovascular medical devices to mitigate thromboembolic and infectious complications. *Adv Healthc Mater* **9**(20): 2001116 (2020)
[35] De Villiers M M, Otto D P, Strydom S J, Lvov Y M. Introduction to nanocoatings produced by layer-by-layer (LbL) self-assembly. *Adv Drug Deliv Rev* **63**(9): 701–715 (2011)
[36] Richardson J J, Cui J W, Björnmalm M, Braunger J A, Ejima H, Caruso F. Innovation in layer-by-layer assembly. *Chem Rev* **116**(23): 14828–14867 (2016)
[37] Sunny S, Vogel N, Howell C, Vu T L, Aizenberg J. Lubricant-infused nanoparticulate coatings assembled by layer-by-layer deposition. *Adv Funct Mater* **24**(42): 6658–6667 (2014)
[38] Lin C X, Wan H P, Kaper H J, Sharma P K. A hyaluronic acid based lubricious coating for cardiovascular catheters. *Tribol Int* **151**: 106495 (2020)
[39] Lin C X, Huang Z Y, Wu T T, Zhou X T, Zhao R F, Xu Z B. A chitosan and hyaluronic acid-modified layer-by-layer lubrication coating for cardiovascular catheter. *Colloids Surf B Biointerfaces* **217**: 112687 (2022)
[40] Wan H P, Ma C, Vinke J, Vissink A, Herrmann A, Sharma P K. Next generation salivary lubrication enhancer derived from recombinant supercharged polypeptides for xerostomia. *ACS Appl Mater Interfaces* **12**(31): 34524–34535 (2020)

[41] Wang Y, Ye C R, Su H, Wang J, Wang Y N, Wang H H, Zhao A S, Huang N. Layer-by-layer self-assembled laminin/fucoidan films: Towards better hemocompatibility and endothelialization. *RSC Adv* **6**(61): 56048–56055 (2016)

[42] Lin C X, Yuan H L, Wang C Y. The study of quantitative friction-damage models at the interventional catheter-vascular tissues interface. *Friction* https://doi.org/10.26599/FRICT.2025.9441194 (2025)

[43] Wan H, Vissink A, Sharma P K. Enhancement in xerostomia patient salivary lubrication using a mucoadhesive. *J Dent Res* **99**(8): 914–921 (2020)

[44] Lin C X, Huang Z Y, Wu T T, Xu W K, Zhao R F, Zhou X T, Xu Z B. Catechol-modified chitosan hydrogel containing PLGA microspheres loaded with triclosan and chlorhexidine: A sustained-release antibacterial system for urinary catheters. *Pharm Dev Technol* **27**(5): 545–553 (2022)

[45] Park J Y, Salmeron M. Fundamental aspects of energy dissipation in friction. *Chem Rev* **114**(1): 677–711 (2014)

[46] Wan H P, Zhao X H, Lin C X, Kaper H J, Sharma P K. Nanostructured coating for biomaterial lubrication through biomacromolecular recruitment. *ACS Appl Mater Interfaces* **12**(21): 23726–23736 (2020)

[47] Neto A I, Cibrão A C, Correia C R, Carvalho R R, Luz G M, Ferrer G G, Botelho G, Picart C, Alves N M, Mano J F. Nanostructured polymeric coatings based on chitosan and dopamine-modified hyaluronic acid for biomedical applications. *Small* **10**(12): 2459–2469 (2014)

[48] Neto A I, Vasconcelos N L, Oliveira S M, Ruiz-Molina D, Mano J F. High-throughput topographic, mechanical, and biological screening of multilayer films containing mussel-inspired biopolymers. *Adv Funct Mater* **26**(16): 2745–2755 (2016)

[49] Wang J, Ma L, Li W, Zhou Z R. Influence of different lubricating fluids on friction trauma of small intestine during enteroscopy. *Tribol Int* **126**: 29–38 (2018)

[50] Wang J, Li W, Wang B R, Zhou Z R. Influence of clamping parameters on the trauma of rabbit small intestine tissue. *Clin Biomech* **70**: 31–39 (2019)

[51] Lin C X, Li W, Deng H Y, Li K, Zhou Z R. Friction behavior of esophageal mucosa under axial and circumferential extension. *Tribol Lett* **67**: 9 (2019)

[52] Salwowska N M, Bebenek K A, Żądło D A, Wcisło-Dziadecka D L. Physiochemical properties and application of hyaluronic acid: A systematic review. *J Cosmet Dermatol* **15**(4): 520–526 (2016)

Chengxiong Lin received his Ph.D. degree in mechanical design and theory from Southwest Jiaotong University in 2020. He is an associate professor from the School of Mechanical Engineering at Wuhan University of Science and Technology. His research interests include biotribology, bio3D printing, and antibacterial lubricating materials.

Huilu Yuan received his bachelor degree and master degree in electromechanical engineering from Guangdong University of Technology in 2021. His research interests include surface engineering and medical devices.

Chengyong Wang received his Ph.D. degree from Dalian University of Technology, China, in 1989. He is a professor and director of the Guangdong Provincial Key Laboratory of Minimally Invasive Surgical Instruments and Manufacturing Technology, Guangdong University of Technology, China. His research interests include machining difficult-to-machine materials and the design and manufacture of medical and surgical tools.